

## Article

# Methodology for Predicting the Structural Response of RPC-Filled Steel Tubular Columns under Blast Loading

Zhizhong Jiang <sup>1,\*</sup>, Qin Rong <sup>1,\*</sup>, Xiaomeng Hou <sup>2,\*</sup> , Zhonghui Zhao <sup>1</sup> and Enyuan Yang <sup>1</sup>

<sup>1</sup> School of Architecture and Civil Engineering, Harbin University of Science and Technology, Harbin 150080, China

<sup>2</sup> Key Lab of Structures Dynamic Behavior and Control of the Ministry of Education, Harbin Institute of Technology, Harbin 150090, China

\* Correspondence: hitrongqin@126.com (Q.R.); houxiaomeng@gmail.com (X.H.)

**Abstract:** Reactive powder concrete-filled steel tube (RPC-FST) is a critical supporting component of large-span, high-rise, and heavy-load structures. The collapse of RPC-FST may occur under explosive load. Therefore, investigation of the dynamic response is essential for understanding the mechanisms of collapse. In this article, the numerical simulation of reactive powder concrete (RPC) adopted the modified Holmquist–Johnson–Cook (HJC) model and the modified Karagozian and Case (K&C) model. The dynamic response of RPC-FST columns under explosive load is analyzed based on arbitrary Lagrange–Euler (ALE) method. The proposed model is verified by experimental results. Results show that the modified HJC model and modified K&C model can be applied to simulate the dynamic response of RPC-FST columns under explosive load. As compared with the modified HJC model, the modified K&C model has more accurate results. This phenomenon mainly accounts for the lack of ultimate strain of RPC (*EFMIN*). To analyze the reliability sensitivity of RPC-FST, an efficient probability analysis method is proposed based on the Kriging model and Monte Carlo simulation (MCS). The proposed method considers five nonlinear factors, including weight and distance of TNT, height and section diameter of RPC-FST, and steel tube thickness. Finally, the sensitivity of each factor is evaluated. Results show that TNT weight greatly influences the reliability of the RPC-FST, followed by TNT distance, RPC-FST height, RPC-FST section diameter, and steel tube thickness. In addition, the RPC-FST dynamic response analysis method based on the Kriging model and MCS can improve the calculation efficiency by more than 200 times compared with the ALE method.

**Keywords:** RPC-FST; dynamic response; modified K&C model; modified HJC model; kriging model; sensitivity analysis



**Citation:** Jiang, Z.; Rong, Q.; Hou, X.; Zhao, Z.; Yang, E. Methodology for Predicting the Structural Response of RPC-Filled Steel Tubular Columns under Blast Loading. *Appl. Sci.* **2022**, *12*, 9142. <https://doi.org/10.3390/app12189142>

Academic Editor: Chao-Wei Tang

Received: 13 August 2022

Accepted: 9 September 2022

Published: 12 September 2022

**Publisher's Note:** MDPI stays neutral with regard to jurisdictional claims in published maps and institutional affiliations.



**Copyright:** © 2022 by the authors. Licensee MDPI, Basel, Switzerland. This article is an open access article distributed under the terms and conditions of the Creative Commons Attribution (CC BY) license (<https://creativecommons.org/licenses/by/4.0/>).

## 1. Introduction

Terrorist activities increased considerably over the past two decades. According to a survey, explosions account for 50% of terrorist attacks, which has raised deep concerns regarding the safety of civilian and military infrastructure [1–3]. Therefore, the evaluation of reactive powder concrete-filled steel tube (RPC-FST) performance and the improvement of RPC-FST reliability under explosive loads are crucial in construction.

The explosion process is a typical nonlinear transient dynamic issue. The methods of applying explosion load are directly related to the accuracy of the numerical analysis. In general, the methods of applying explosion load can be roughly divided into three types: arbitrary Lagrange–Euler (ALE), load blast enhanced (LBE), and pressure-time history method. Among these, the LBE-based method defines explosion load based on the empirical blast loading function, which is derived from experimental explosion data [4,5]. Compared with the LBE-based method, the pressure-time history method defines the explosion load according to an exponentially decaying function (such as Friedlander's equation), which can be replaced with an equivalent triangular function when the negative

phase effect can be ignored [6,7]. The LBE-based method and pressure-time history method have high computational efficiency. Nevertheless, these simplified methods lack a profound understanding of the functional mechanism between air and RPC-FST. Contrary to the aforementioned methods, the ALE-based method can accurately restore local details of blast conditions considering fluid–solid interaction (FSI) theory. Based on this method, Thai [8] assessed the residual strength of fiber-reinforced concrete columns under explosion load. Kostopoulos [9] investigated the blast resistance of a composite foam-core sacrificial cladding for steel-reinforced concrete structures. Wu [10] investigated the dynamic response of ultra-high-performance cement-based composite-filled steel tube (UHPCC-FST) under close-range explosion.

Besides the methods of applying explosion load, the material model is also a significant factor in precisely simulating the dynamic response of a structure under explosion load. The LS-DYNA program offers many dynamic constitutive models for simulating concrete materials, such as the Holmquist–Johnson–Cook (HJC) model and the Karagozian and Case (K&C) model. The HJC model is mainly suitable for material under large strain, high strain rate, and high pressure [11]. Based on the HJC material model, Zhu [12] established a theoretical model for shaped charge jets' penetration into concrete targets. Kristoffersen [13] investigated the ballistic perforation resistance of concrete slabs. Wan [14] calibrated parameters to investigate the blast resistance of ultra-high-performance concrete (UHPCs) slabs. It should be noted that the modified HJC model parameters are suitable for UHPCs slabs with 10.5% porosity of coarse aggregate. However, the applicability of HJC material model parameters modified for RPC materials with low porosity without coarse aggregate needs to be deeply investigated.

Different from the HJC material model, the K&C material model has great advantages in describing the material under damage evolution, restraint effect, and shear expansion [15]. Based on the K&C material model, Wang [16] estimated the residual axial load-bearing capacity of UHPCC-FST specimens subjected to contact explosion. Liu [17] investigated the damage evolution of reinforced concrete piers with carbon-fiber-reinforced polymer under contact explosion. Zhang [18] calibrated the model parameters of UHPCs with high-velocity projectile impact experimental data. Meanwhile, reactive powder concrete (RPC) is a low-porosity material due to its dense microstructure [19]. However, the calculation accuracies of the HJC material model and K&C material model have not been deeply investigated for RPC with low porosity. Therefore, the application scopes of the K&C material model and HJC material model require more discussion.

There are still many challenges in calculating the dynamic response of RPC-FST columns under explosion loads. The correct description of the RPC material model under steel tube constraint has research value. In addition, the influence of different types of fiber and different fiber contents in RPC on the dynamic response of an RPC-FST column under explosion load is still worth discussing. Although most scholars have investigated the mechanical properties of RPC-FST with experiments [20–22], the changes in the mechanical properties of RPC-FST columns under explosion loads are not clear. Therefore, dynamic response analysis of RPC-FST columns under explosion load is still in the exploratory stage.

In practical scenarios, it is impossible to accurately describe and deterministically control the nonlinear factors of the explosion process. Therefore, the characteristic parameters for estimating the stability of the RPC-FST are random. For example, manufacturing error causes randomness in the dimensions of the RPC-FST column. Moreover, the randomness of weight and distance of TNT cause uncertainty of the explosion load. Therefore, it is critical to establish the probability analysis for the explosion process. Hussein [23] investigated the reliability of composite wood-sand-wood blast walls based on Monte Carlo simulation (MCS). Song [24] presented the reliability analysis method for a steel frame structure under explosion load based on Bayesian theory. Ding [25] established an effective reliability evaluation framework to predict the failure risk of steel frame structures under explosion load. Shi [26] predicted the damage of reinforced concrete wall panels under various threats based on MCS. Momeni [27] presented an improved calculation method,

based on the MCS method and finite element approach, to evaluate the minimum safe scaled distance for steel columns under dynamic blast loads. Beyond any dispute, the application of these above methods can provide guidance for the probability analysis of the explosion process. Nevertheless, the reliability sensitivity analysis of the RPC-FST column based on MCS still requires further investigation.

In this article, the critical axial deformation is employed as the stability threshold of RPC-FST. Meanwhile, the application scopes of the K&C material model and HJC material model are theoretically illustrated with numerical calculation. To improve the computational efficiency of sensitivity assessment, the surrogate Kriging model is adopted to replace the modified K&C model. The rest of this paper is organized as follows: In Section 2, the explosion load is applied based on the ALE method. In addition, the modified K&C material model for low-porosity RPC materials is established. In Section 3, it is verified that the modified K&C model has advantages over the modified HJC model in material properties of low-porosity RPC. In addition, a numerical example establishes the basis for the Kriging model. In Section 4, the RPC-FST sensitivity analysis of the random explosion process is proposed. The sensitivity of the output with respect to each factor is evaluated.

## 2. RPC-FST Model Based on ALE Method

As the core component of blast-resistant structures, RPC-FST plays a significant role in protecting buildings in explosively hazardous areas from fatal damage. Therefore, the dynamic response of RPC-FST under explosive load has attracted wide attention. In the process of dynamic response analysis, the robustness of the model directly affects the accuracy of numerical calculation. In this section, the K&C model is modified based on the low porosity of RPC material. In addition, the finite element model (FEM) of RPC-FST under explosion load is established based on the ALE method, as shown in Figure 1.

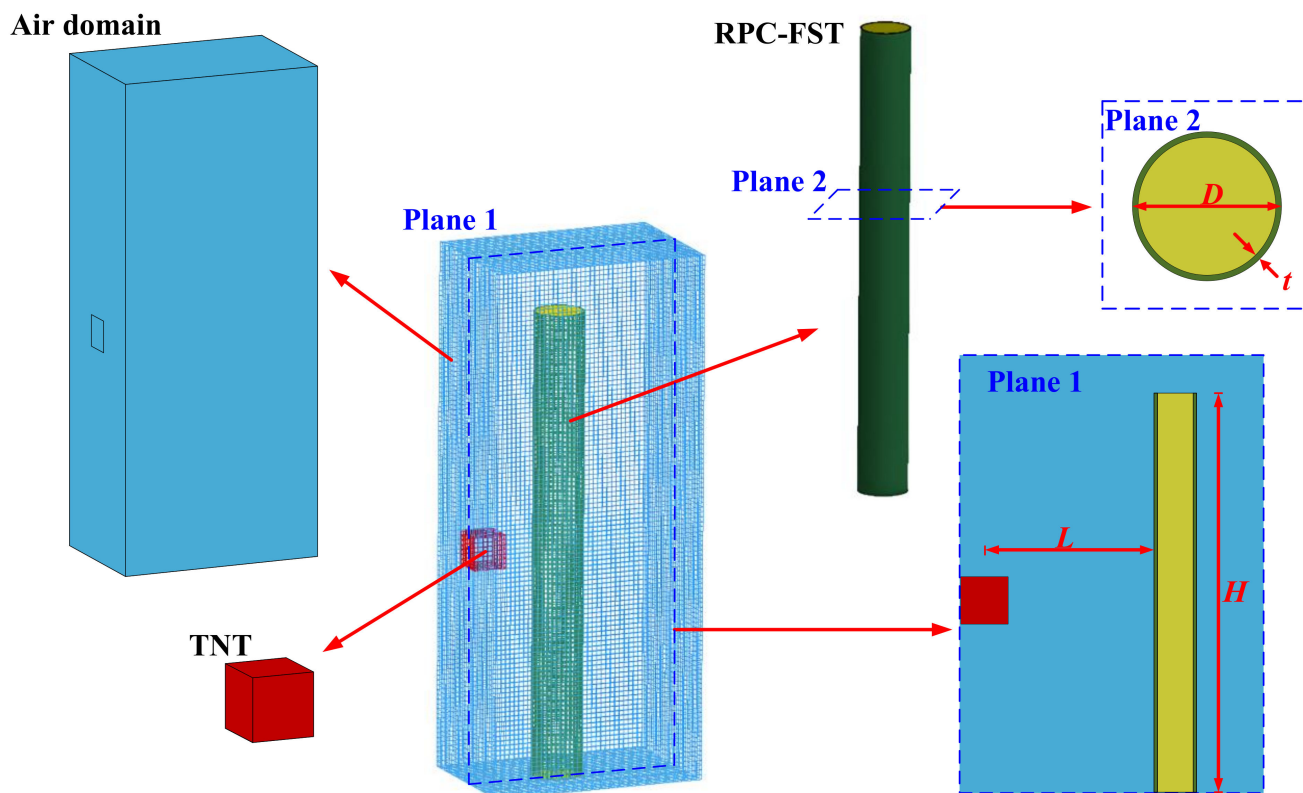


Figure 1. Finite element model based on ALE method.

### 2.1. Fluid–Solid Interaction of RPC-FST

The approach for solving FSI problems is the ALE formulation for the fluid domain and the Lagrangian formulation for the structure domain. This approach is called the ALE method, and it has been intensively used for problems involving small and large structure displacements with no topological changes in the structure. Therefore, the ALE method from LS-DYNA provides a possibility to model multi-phase highly dynamic problems. The nonlinear dynamic analysis program LS-DYNA is used to analyze the dynamic response of RPC-FST columns under explosion load. A numerical model composed of four parts is established. The TNT and air domain are treated as ALE parts, while the RPC-FST columns are treated as Lagrangian parts.

### 2.2. Establishing the Model

The Jones–Wilkins–Lee equation of state (JWL EOS) defines the pressure as a function of the relative volume  $V$  and internal energy  $E_0$ . TNT has been established as material by using the JWL EOS method. It can be expressed as:

$$P = A\left(1 - \frac{\omega}{R_1 V}\right)e^{-R_1 V} + B\left(1 - \frac{\omega}{R_2 V}\right)e^{-R_2 V} + \frac{\omega E_0}{V} \quad (1)$$

where  $A$ ,  $B$ ,  $R_1$ ,  $R_2$ , and  $\omega$  are the parameters related to the TNT type.

The air domain is established with the equation of state, which represents the relationship between the element pressure and the internal energy given in Equation (2).

$$P = C_0 + C_1\mu + C_2\mu^2 + C_3\mu^3 + (C_4 + C_5\mu + C_6\mu^2)E \quad (2)$$

where  $P$  is the pressure,  $C_i$  ( $i = 1, 2, \dots, 6$ ) values are constant, and  $E$  is the internal energy per unit volume.

The plastic kinematic model is an elastic-plastic model with kinematic and isotropic hardening. Therefore, the plastic kinematic model is selected for steel tube materials under impact load. The strain rate effect on steel material can be incorporated by the Cowper and Symonds (CS) model (Equation (3)), which scales the yield stress with the factor.

$$DIF = 1 + \left(\frac{\dot{\epsilon}}{C}\right)^{1/p} \quad (3)$$

where  $\dot{\epsilon}$  is the strain rate.  $C$  and  $p$  denote strain rate parameters for the CS strain rate model. In this study,  $C$  and  $p$  are set as  $6844 \text{ s}^{-1}$  and  $3.91$ , respectively. This combination accurately predicts the dynamic response of concrete-filled steel tubular columns, as verified by tensile experiments [28]. The constants mentioned above will be explained in detail later in Section 3.

RPC has extremely high compressive strength and fracture energy [29–31]. There is a lack of accurate model parameters to describe the characteristics of RPC materials in RPC-FST columns. The K&C model is considered a promising dynamic constitutive model [15], and thus can be used to reveal the material properties under impact and explosion loads. The K&C model is modified according to the characteristics of RPC without coarse aggregate.

The K&C model is specifically used to calculate the concrete structural response under blast and impact loadings. It is comprised of two parts—volume response and deviatoric response.

In volume response, the volume change of materials under different pressures is observed by applying stress. The equation of state \*EOS\_TABULATED\_COMPRESSION correlates the pressure  $p$  and the volumetric strain  $\epsilon_V$ . In deviatoric response, three failure surface strength models—yield failure surface  $\Delta\sigma_y$ , maximum failure surface  $\Delta\sigma_m$ , and residual failure surface  $\Delta\sigma_r$ —have to be characterized via  $a_{0y}$ ,  $a_{1y}$ ,  $a_{2y}$ ,  $a_0$ ,  $a_1$ ,  $a_2$ ,  $a_{1f}$ , and  $a_{2f}$ . The deviatoric stresses remain elastic during loading or reloading until the stress

achieves the yield failure surface. Then, the deviatoric stress further increases until the maximum failure surface is reached. Beyond this stage, the response can be perfectly plastic or softened to the residual failure surface. The damage function captures the hardening and softening behavior of three failure surfaces. According to the characteristics of 5% porosity of RPC material in RPC-FST, the modified K&C model process is shown in Figure 2.

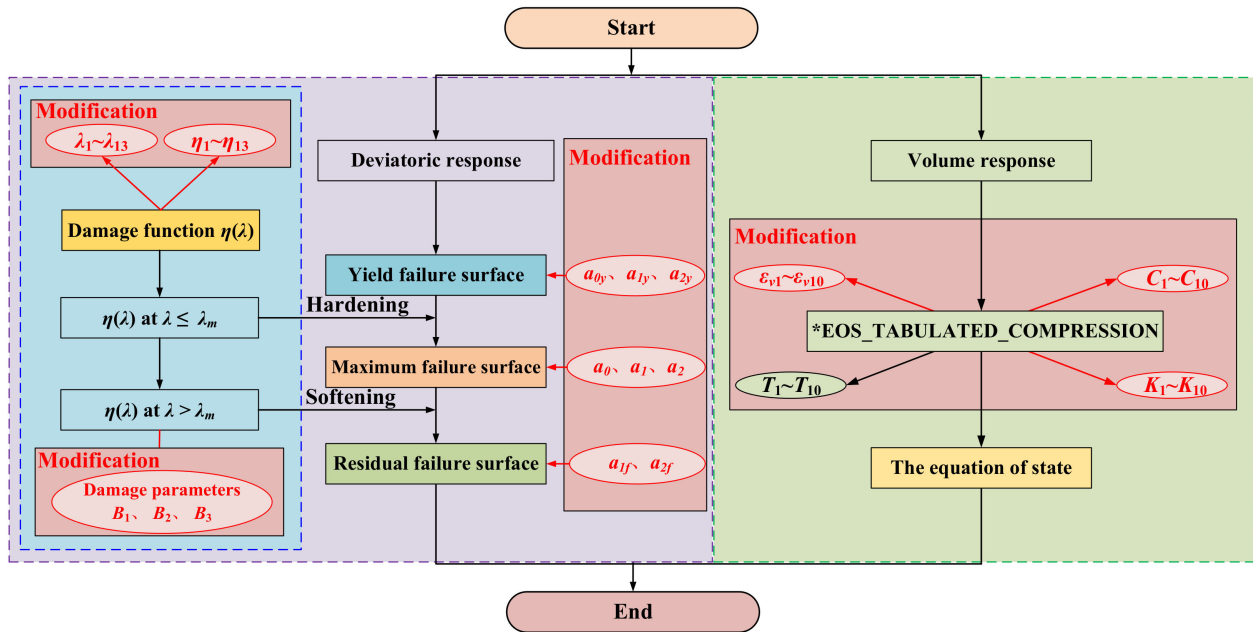


Figure 2. Modified K&C model process.

The dynamic increase factor (*DIF*) relationship proposed by Hou [32] is adopted, which considers the strain rate effect of RPC. The *DIF* of the RPC compressive strength can be expressed as in Equation (4).

$$DIF = a \left( \frac{\dot{\epsilon}}{\dot{\epsilon}_s} \right)^b [\dot{\epsilon}] \leq \dot{\epsilon} \leq 317s^{-1} \quad (4)$$

where  $(\dot{\epsilon})$  is the critical strain rate of *DIF*. If the strain rate is lower than  $(\dot{\epsilon})$ , the strain rate effect on the compressive strength can be neglected. Moreover,  $(\dot{\epsilon}_s) = 1 \text{ s}^{-1}$  is used to make indexes dimensionless, where  $(\dot{\epsilon})$ ,  $a$ , and  $b$  are the constant coefficients for RPC.  $a$  and  $b$  are set as 0.291 and 0.310, respectively.

It is worth noting that detonation products are transmitted in the air with high-frequency shock waves, and their physical process and dynamic response are exceedingly complex. To reveal this process accurately, the determination of air domain size is essential. According to TNT distance, TNT size, RPC-FST, and other model parameters in the practical project, the high-frequency shock wave shows a large amplitude, and the behavior of RPC-FST displacement is geometrically nonlinear. Therefore, the size of the air domain was chosen as 3000 mm × 1000 mm × 8000 mm. The non-reflection boundary keyword is used for air boundary conditions to prevent wave reflection from the boundary. The mesh size denotes 20 mm, and the termination time denotes 50 ms.

### 3. Model Validation and Numerical Examples

In this section, it will be revealed that the modified K&C model has advantages over the modified HJC model for the description of low-porosity RPC material properties in RPC-FST under explosion load. Modified parameters of the K&C model, damage function  $\eta(\lambda)$ , and equation of state are shown in Tables 1–3 [18]. The modified HJC model is shown in Appendix A. Air equation of state parameters are shown in Table 4. The parameters of TNT are shown in Table 5. The material properties of the steel tube are shown in Table 6.

**Table 1.** Modified K&C model parameters.

Parameter	Value	Parameter	Value
Mass density $R_0$ (g/mm <sup>3</sup> )	0.002	Poisson’s ratio $PR$	0.2
Uniaxial tensile strength $T$ (MPa)	9	Failure surface parameter $a_0$	$3.3 \times 10^7$
Failure surface parameter $a_1$	0.45	Failure surface parameter $a_2$	$7.4 \times 10^{-10}$
Compressive damage parameter $B_1$	1.6	Tensile damage scaling exponent $B_2$	1.4
Damage scaling coefficient $B_3$	1.15	Initial yield surface coefficient $a_{0y}$	$2.5 \times 10^7$
Initial yield surface coefficient $a_{1y}$	0.63	Initial yield surface coefficient $a_{2y}$	$2.3 \times 10^{-9}$
Residual failure surface coefficient $a_{1f}$	0.44	Residual failure surface coefficient $a_{2f}$	$1.1 \times 10^{-9}$
Aggregate diameter $LOCWID$ (mm)	0.03	Post peak dilatancy decay $EDROP$	1
Stretch factor $S_\lambda$	100	Fractional dilatancy $OMEGA$	0.5
Unit conversion for length $R_{SIZE}$	0.04	Unit conversion for stress $UCF$	145

**Table 2.** Modified damage function  $\eta(\lambda)$ .

Scale Factor $\lambda$				Damage Function $\eta$			
Parameter	Value	Parameter	Value	Parameter	Value	Parameter	Value
$\lambda_1$	0	$\lambda_8$	$3.2 \times 10^{-4}$	$\eta_1$	0	$\eta_8$	0.85
$\lambda_2$	$8.0 \times 10^{-6}$	$\lambda_9$	$5.2 \times 10^{-4}$	$\eta_2$	0.85	$\eta_9$	0.67
$\lambda_3$	$2.4 \times 10^{-5}$	$\lambda_{10}$	$5.7 \times 10^{-4}$	$\eta_3$	0.97	$\eta_{10}$	0.57
$\lambda_4$	$4.0 \times 10^{-5}$	$\lambda_{11}$	1	$\eta_4$	0.99	$\eta_{11}$	0.37
$\lambda_5$	$5.6 \times 10^{-5}$	$\lambda_{12}$	$1.0 \times 10^1$	$\eta_5$	1	$\eta_{12}$	0.37
$\lambda_6$	$7.2 \times 10^{-5}$	$\lambda_{13}$	$1.0 \times 10^{10}$	$\eta_6$	0.99	$\eta_{13}$	0.37
$\lambda_7$	$8.8 \times 10^{-5}$			$\eta_7$	0.97		

**Table 3.** Modified equation of state.

Volumetric Strain		Pressure		Bulk Unloading Modulus	
Parameter	Value	Parameter	Value (MPa)	Parameter	Value (MPa)
$\epsilon_{v1}$	0	$C_1$	0	$K_1$	20,540
$\epsilon_{v2}$	0.0015	$C_2$	30.81	$K_2$	20,541
$\epsilon_{v3}$	0.002	$C_3$	39.43	$K_3$	20,830
$\epsilon_{v4}$	0.0025	$C_4$	49.03	$K_4$	21,870
$\epsilon_{v5}$	0.0029	$C_5$	73.05	$K_5$	26,020
$\epsilon_{v6}$	0.0043	$C_6$	94.94	$K_6$	30,190
$\epsilon_{v7}$	0.0101	$C_7$	103.32	$K_7$	34,340
$\epsilon_{v8}$	0.0305	$C_8$	196.3	$K_8$	37,480
$\epsilon_{v9}$	0.0513	$C_9$	296.08	$K_9$	84,330
$\epsilon_{v10}$	0.0726	$C_{10}$	420.06	$K_{10}$	102,700

**Table 4.** Air equation of state parameters.

Parameter	$C_0$	$C_1$	$C_2$	$C_3$	$C_4$	$C_5$	$C_6$	$E$ (J/mm <sup>3</sup> )	$V$
Value	0	0	0	0	0.4	0.4	0	0.3	1

**Table 5.** TNT parameters.

Parameter	Value	Parameter	Value
TNT density $R_0$ (g/mm <sup>3</sup> )	$1.63 \times 10^{-3}$	Detonation velocity $D$ (m/s)	$6.93 \times 10^3$
Parameter $A$	$3.71 \times 10^5$	Parameter $B$	$3.23 \times 10^3$
Parameter $R_1$	4.15	Parameter $R_2$	0.95
Parameter $w$	0.3	Detonation energy $E_0$ (J/mm <sup>3</sup> )	7000
Initial relative volume $V$	1	Chapman-Jouget pressure $PCJ$	$2.70 \times 10^4$

**Table 6.** Material properties of steel tube.

Parameter	Value	Parameter	Value
Mass density $R$ (g/mm <sup>3</sup> )	$7.85 \times 10^{-3}$	Young's modulus $E$ (MPa)	$2.05 \times 10^5$
Poisson's ratio $PR$	0.3	Yield stress $SIGY$ (MPa)	318.5
Hardening parameter $BETA$	0	Strain rate parameter $SRC$	6844
Effective plastic strain $FS$	0.25	Strain rate parameter $SRP$	3.91

3.1. Model Competition

In order to profoundly investigate the accuracy of the modified K&C model and the modified HJC model, we decided to verify the applicability of the two modified material models to RPC materials according to the explosion experiment conducted by Wang [33] in the recent report. The compressive strength of RPC is 135.1 MPa, and steel tube yield strength is 318.5 MPa. The top of the column limits the displacement in the  $x$ ,  $y$ , and  $z$  directions, and the bottom end is a fixed-end constraint. Model parameters are shown in Table 7.

**Table 7.** Model parameters.

Specimen	TNT Weight (kg)	TNT Height (mm)	TNT Distance (mm)	Steel Tube Thickness (mm)
C-15	4	250	221	6
C-16	4	950	221	6
C-17	7	955	230	6
C-18	10	945	275	6

The modified K&C model, HJC model, modified HJC model, and experiment comparison are shown in Figure 3. Among them, the material parameters of the HJC material model are determined according to Wan [14]. It should be pointed out that the residual displacement results of the experiments are used for the verification. The results show that the modified K&C model parameters have better accuracy in calculating dynamic response than the modified HJC model parameters and parameters of the modified HJC model proposed by Wan [14]. The displacement time history curve of the modified K&C model converges to the experimental value faster through vibration. The increase of RPC damage degree in RPC-FST under near-range explosion load is the main reason for the inaccurate numerical calculation.

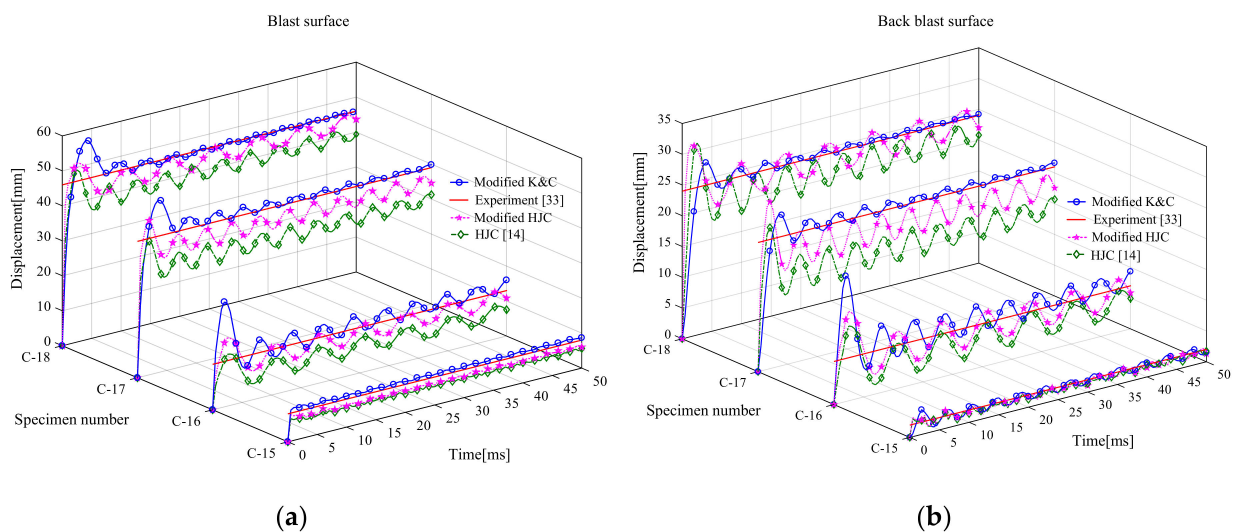


**Figure 3.** Modified K&C model, HJC model, modified HJC model, and experiment comparison: (a) blast surface displacement of RPC-FST and (b) back blast surface displacement of RPC-FST.

The structural response under explosion loading is influenced by the constitutive models of the material, which will bring uncertainty to structural protection. The result of residual displacement with the HJC model is obviously lower than the experimental value. This phenomenon is mainly because the parameters are modified for RPC containing coarse aggregate [14]. The porosity of RPC containing coarse aggregate is generally 10.5%, while the porosity of RPC without coarse aggregate is generally 5%, which leads to a certain deviation in the expression of the equation of state under this working condition. In addition, determining the parameters of the damage evolution equation based only on steel fiber content needs to be further discussed. Therefore, the dynamic response analysis of the modified HJC model is carried out. The results show that the modified HJC model has obvious advantages over the HJC model. This phenomenon is mainly because the modified HJC model considers the influence of porosity on the equation of state. Furthermore, the effects of the water/cement ratio, steel fiber content, and steel fiber length on the damage evolution equation are considered. However, the advantages of the modified K&C model are still obvious. Through analysis, it should be pointed out that the slope of the assumed failure surface is characterized by uncertainty, the values of ultimate strains  $\epsilon_x$  obtained by the uniaxial compression test are too large, and the damage parameter  $D$  is small (Figure A2). Therefore, the deviation of the damage evolution equation leads to the calculation results of the HJC model being lower than the experiment results.

From Figure 4, it is found that the dynamic responses of RPC-FST calculated based on the modified K&C model are consistent with the experimental results. From the experiment, the steel tube surface of the crater exhibited many tiny scars. The results show that some elements fail on the blast surface, which is consistent with the experimental phenomenon. Due to some solid elements of steel tube reaching ultimate strength after bearing the explosion load and being unable to continue bearing the load, the result is solid element failure.

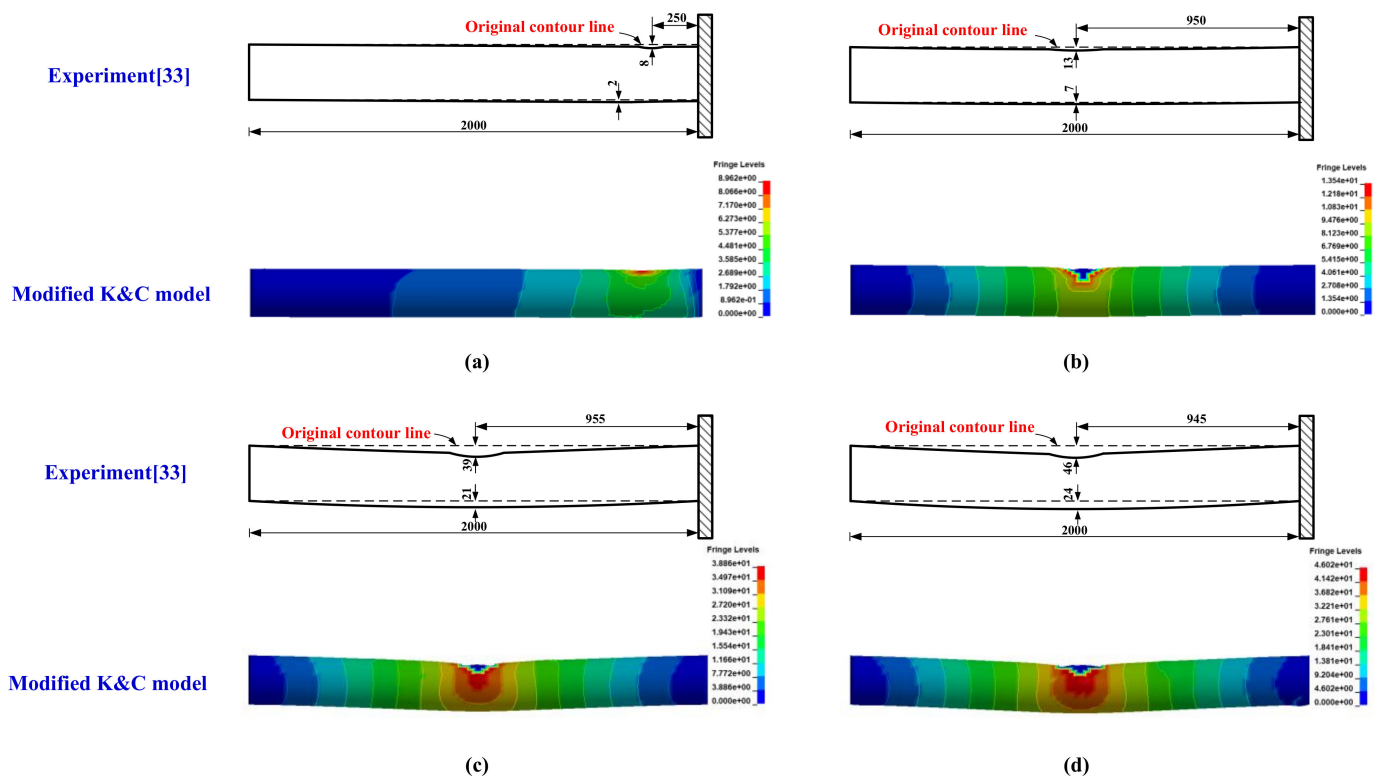


Figure 4. Comparison of blast surface displacement between experiment and numerical simulation (mm): (a) C-15, (b) C-16, (c) C-17, and (d) C-18.

### 3.2. Numerical Example

According to the model comparison, it is found that the modified K&C model is more suitable for the RPC material model in RPC-FST. Therefore, the RPC material model is established by using the modified K&C model. In addition, a group of samples after the Latin hypercube sampling plan is selected as the structural parameters of RPC-FST. This process establishes the basis for the reliability sensitivity analysis of RPC-FST in Section 4. The dynamic response analysis of the RPC-FST column under explosive load is carried out based on FSI theory. The bottom and top of the RPC-FST columns are restrained in the  $x$ ,  $y$ , and  $z$  directions, whereas all the other degrees of freedom can move freely.

The ALE method can evaluate a blast scenario with more detail, including explosive detonation. Therefore, the velocity of the shock wave and the displacement of RPC-FST are extracted. Figure 5 illustrates the functional mechanism between air and RPC-FST.

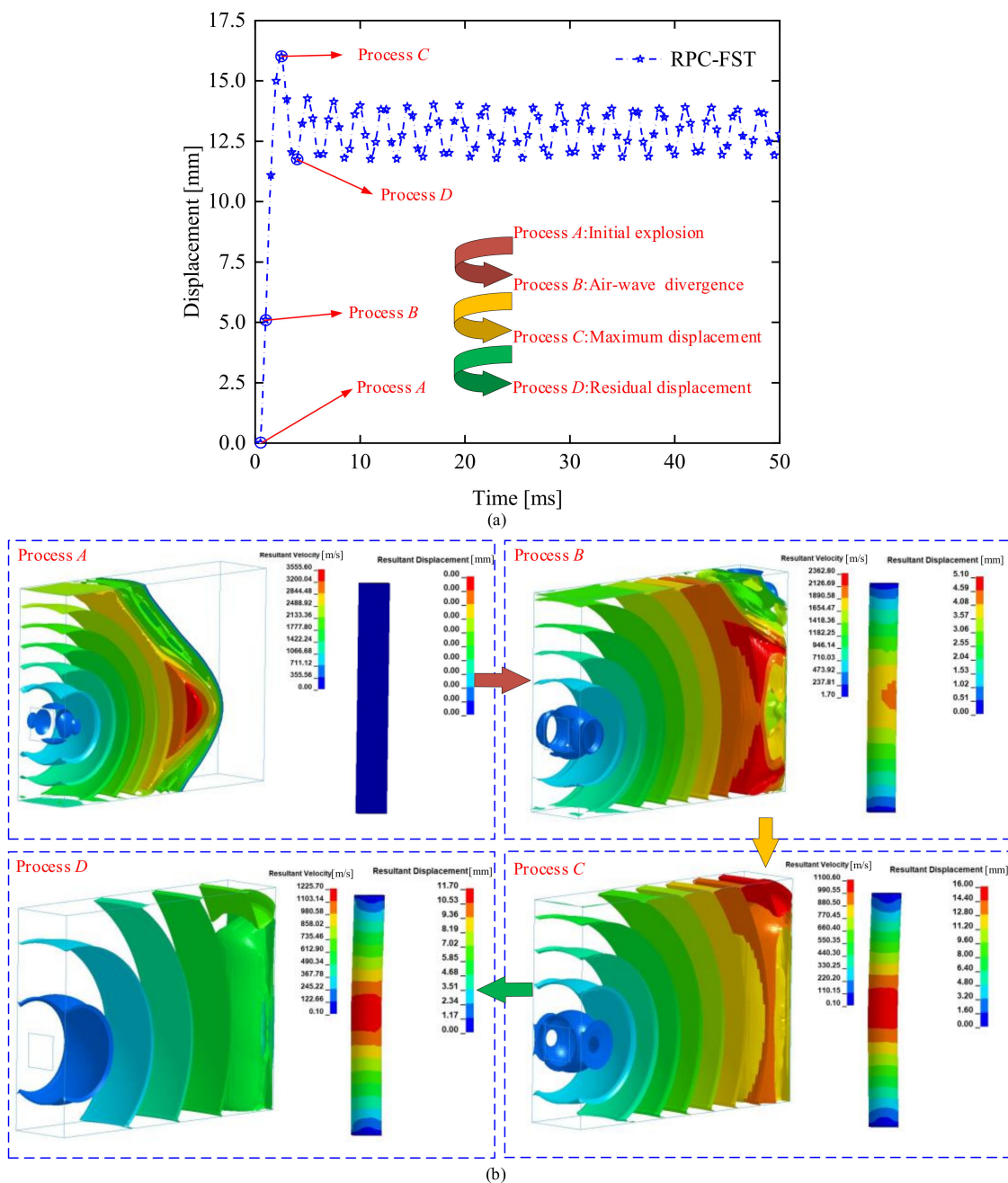


Figure 5. Explosive process analysis of a numerical example: (a) four processes of explosion and (b) details of each process.

The evolutions of RPC-FST dynamic response under explosion load can be roughly divided into four phases: process A, process B, process C, and process D, as shown in Figure 5a. Meanwhile, the details of each process are shown in Figure 5b. The results show that the shock wave did not reach the blast surface of RPC-FST at 0.5 ms. The maximum displacement of the RPC-FST occurred at 2.5 ms. In addition, the maximum displacement (process C) in the RPC-FST displacement time history curve is selected to establish the Kriging surrogate model.

#### 4. Sensitivity Analysis of RPC-FST

Irreversible RPC-FST damage will emerge during the explosion process. Meanwhile, the accumulation of the damage process will decrease the durability of the RPC-FST [22]. Furthermore, the characteristic parameters for estimating the damage of the RPC-FST are random due to manufacturing and measurement errors [34,35]. Therefore, the quantification and propagation of randomness of the explosion process are critical in RPC-FST design. In addition, the low calculation efficiency of the modified K&C model under explosion load is considered. The surrogate Kriging model is adopted to replace the modified K&C model for sensitivity analysis of RPC-FST under random explosion load.

For probabilistic analysis, the reliability of RPC-FST under explosion load can be defined as a multi-dimensional integral:

$$P_s = \int \cdots \int_{G(x)>0} f_X(x) dx \tag{5}$$

where

$$G(x) = \left[ \left( \frac{H}{2} \right) \times \tan(\theta) \right] - \varepsilon(x) \tag{6}$$

where  $G(x)$  is the limit state function, which can be established based on Section 2;  $x = (H, W, t, L, D)^T$  is a vector of independent random variables used to calculate the dynamic response of the RPC-FST system;  $X$  is a random parameter vector corresponding to  $x$ ;  $H$  is the height of RPC-FST;  $W$  is the weight of TNT;  $t$  describes the thickness of steel tube;  $L$  represents the distance between TNT and RPC-FST;  $D$  is the section diameter of RPC-FST; and  $\theta$  denotes the deflection angle of RPC-FST at the upper damage limit [36]. According to TM5-1300 [3], the damage levels of concrete-filled steel tube columns can be divided into low damage, moderate damage, and high damage (Table 8). Therefore, the failure probability is calculated for the low damage of a 0–2° column, as shown in Figure 6. In order to calculate the sensitivity of the allowable deflection angle between 0 and 2°, we decided to choose 1.4° as the allowable deflection angle.  $\varepsilon(x)$  is the maximum displacement based on FSI theory. However, due to the high dimensionality and complicated integrand of Equation (5), both analytical and direct numerical methods cannot be applied directly.

**Table 8.** Damage level of concrete-filled steel tube column.

Damage Level	Low Damage	Moderate Damage	High Damage
$\theta$	0–2°	2–5°	5–12°

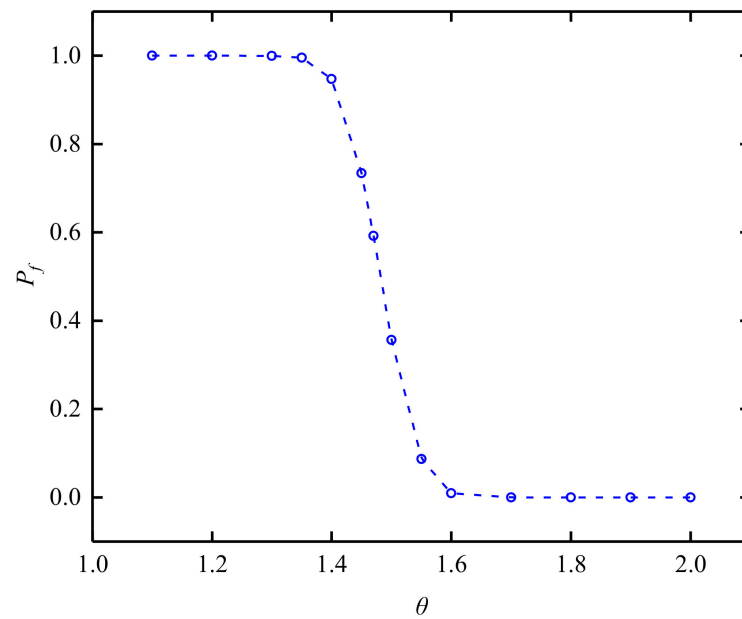


**Figure 6.** Failure probability  $P_f$  of RPC-FST at different allowable deflection angles  $\theta$ .

4.1. Monte Carlo Simulation (MCS) Method

MCS is an accurate technique to solve complex multi-dimensional integrals [37]. The problem solution is transformed into the expectation of the probability model. Meanwhile, statistical analysis is adopted to evaluate the probability approximation of the multi-dimensional integral [38]. The conversion of Equation (5) based on MCS can be expressed as:

$$P_f = \int_F I_F(x) f_X(x) dx = E(I_F(x)) \tag{7}$$

where  $F$  is the failure domain of RPC-FST, and  $I_F(x)$  is the indication function of the failure domain, which can be obtained by:

$$I_F(X) = \begin{cases} 0 & G(X) > 0 \\ 1 & G(X) \leq 0 \end{cases} \tag{8}$$

Therefore, the failure probability of RPC-FST can be calculated by:

$$P_f = \frac{1}{N} \sum_{j=1}^N E(I_F(x_j)) \approx \frac{1}{N} \sum_{j=1}^N I_F(x_j) \tag{9}$$

4.2. Sensitivity Analysis Based on Kriging

To ensure the accuracy of the reliability sensitivity analysis for RPC-FST based on MCS, numerous repeatability calculations should be completed. However, the limit state function Equation (6) is highly complex and implicit. Therefore, the reliability sensitivity analysis for RPC-FST is limited by its high computational cost. To improve the calculation efficiency of the limit state function, the surrogate model Kriging is adopted to establish an approximation form for  $G(x)$ .

The surrogate Kriging model was created from an initial number of computational RPC-FST dynamic response calculations in a design of experiments (DoE) sampling plan. There exist several DoE techniques, and in this work, the Latin hypercube sampling (LHS) plan was used. The LHS plan divides each design parameter into  $N$  equally sized intervals, where the same value of a parameter can only occur once [39]. TNT weight, TNT distance, steel tube thickness, RPC-FST diameter, and RPC-FST height are five design parameters. An example of a randomly generated LHS plan can be seen in Figure 7.

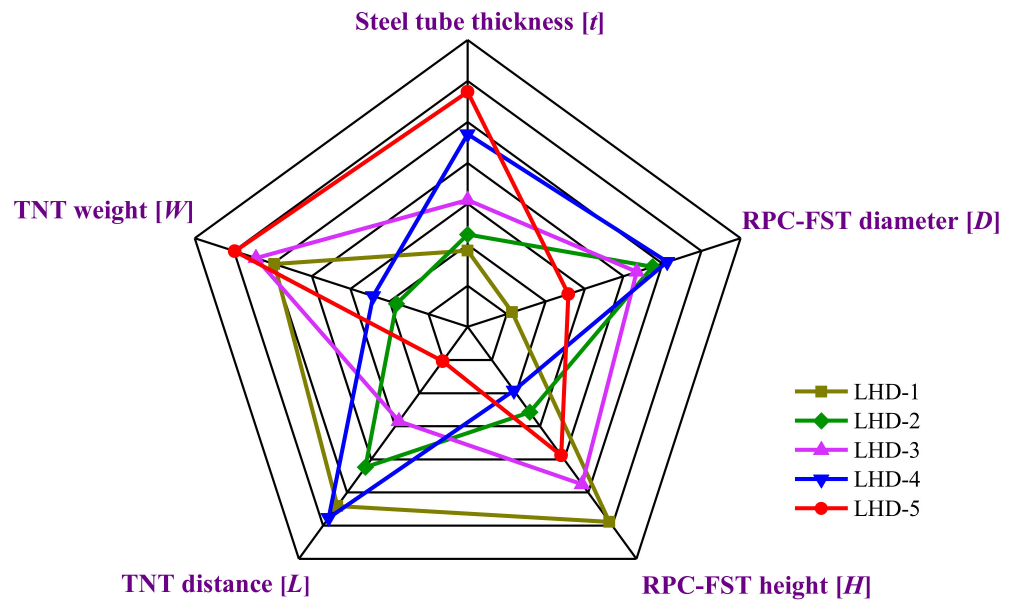


Figure 7. An example of a randomly generated LHS plan.

The basic idea of the Kriging method includes two parts: a regression model used to represent the global trend and a stochastic process used to represent the local behavior [40]. Therefore, the Kriging model can be expressed as Equation (10).

$$g_k(X) = \sum_{i=1}^p f_i(X)\beta_i + z(X) \tag{10}$$

where  $f(X) = \{f_1(X), f_2(X), \dots, f_p(X)\}^T$  is the vector of regression basis functions;  $\beta = \{\beta_1, \beta_2, \dots, \beta_p\}^T$  is the vector of the regression coefficients;  $p$  is the number of the basic functions in the regression model; and  $z(X)$  is assumed to be a Gaussian stationary process with a mean of zero and a standard deviation of  $\sigma$ . The covariance matrix can be expressed as:

$$\text{cov}[z(X^{(i)}), z(X^{(j)})] = \sigma^2[R(X^{(i)}, X^{(j)}, \theta)] \tag{11}$$

where  $R(X^{(i)}, X^{(j)})$  is the spatial auto-correlation function between input samples  $X^{(i)}$  and  $X^{(j)}$ , which coordinates the smoothness of the Gaussian model. It can be expressed as:

$$R[X^{(i)}, X^{(j)}, \theta] = \exp\left(-\sum_{k=1}^m \theta_k \left|X_k^{(i)} - X_k^{(j)}\right|^2\right) \tag{12}$$

where  $\theta = \{\theta_1, \theta_2, \dots, \theta_k\}^T$  is a hyperparameters vector defining the auto-correlation function. The hyperparameters vector  $\theta$  can be estimated as follows using the maximum likelihood method:

$$\max F(\theta) = -\frac{m \ln(\hat{\sigma}^2) + \ln(R)}{2} \theta_k \geq 0 \tag{13}$$

where

$$\begin{cases} \hat{\sigma}^2 = (g - F_k \hat{\beta})^T R^{-1} (g - F_k \hat{\beta}) / m \\ \hat{\beta} = (F_k^T R^{-1} F_k)^{-1} F_k^T R^{-1} g \end{cases} \tag{14}$$

where  $\hat{\sigma}^2$  is an estimate of  $\sigma$ ;  $\hat{\beta}$  is an estimate of  $\beta$ ;  $F_k$  is a matrix, which gathers the regression functions based on training points; and  $g$  is the response vector corresponding to training points. The predicted response vector of the Kriging model at a given unknown point  $X$  can be expressed as:

$$g_k(X) = f^T(X)\hat{\beta} + r^T(X)R^{-1}(g - F\hat{\beta}) \tag{15}$$

where  $r(X)$  is the correlation vector between the training and predicting points. It can be expressed as:

$$r^T(X) = \{R(X, X^{(1)}), R(X, X^{(2)}) \dots R(X, X^{(m)})\} \tag{16}$$

The predictive mean and variance for the Kriging model can be performed as follows:

$$\begin{aligned} \mu_{gk}(X) &= f^T(X)\hat{\beta} + r^T(X)R^{-1}(g - F\hat{\beta}) \\ \sigma^2_{gk}(X) &= \hat{\sigma}^2 \left\{ 1 - r^T(X)R^{-1}r(X) + [F^T R^{-1}r(X) - f(X)]^T (F^T R^{-1}F)^{-1} [F^T R^{-1}r(X) - f(X)] \right\} \end{aligned} \tag{17}$$

To make the output Kriging surrogate model more accurately predict the displacement of the RPC-FST column, the relative error-index  $\beta_R$  (Equation (18)) is used to evaluate the model [41].

$$\beta_R = \frac{g_k(X_L) - g_L(X_L)}{g_L(X_L)} \tag{18}$$

where  $X_L$  is a variable matrix composed of  $N_L$  samples generated by the LHS plan,  $g_k(X_L)$  is the output by the updated Kriging surrogate model, and  $g_L(X_L)$  is the output by the theory of FSI analysis.

Based on the MCS method, the reliability can be expressed as:

$$\frac{\partial P_f}{\partial \theta_{X_i}^{(k)}} = \int \dots \int_{R^n} I_F(x) \frac{\partial f_X(x)}{\partial \theta_{X_i}^{(k)}} \frac{1}{f_X(x)} f_X(x) dx = E \left[ \frac{I_F(x)}{f_X(x)} \frac{\partial f_X(x)}{\partial \theta_{X_i}^{(k)}} \right] \tag{19}$$

The reliability sensitivity is obtained as Equation (20).

$$\beta_S = \frac{\partial P_f}{\partial \theta_{X_i}^{(k)}} = \frac{1}{N_{MC}} \sum_{j=1}^{N_{MC}} \frac{I_F(X)}{f_X(X)} \frac{\partial f_X(X)}{\partial \theta_{X_i}^{(k)}} \tag{20}$$

The sensitivity coefficient is calculated as follows:

$$\text{cov}(\beta_S) \approx \sqrt{\frac{\frac{1}{N_{MC}-1} \left( \frac{1}{N_{MC}} \sum_{j=1}^{N_{MC}} \left[ \frac{I_F(X)}{f_X(X)} \frac{\partial f_X(X)}{\partial \theta_{X_i}^{(k)}} \right]^2 - (\beta_S)^2 \right)}{|\beta_S|}} \tag{21}$$

The sensitivity of the five input variables of steel tube thickness, RPC-FST column height, TNT weight, TNT distance, RPC-FST section diameter to the displacement error risk of RPC-FST columns, and sensitivity coefficient are evaluated by Equations (20) and (21). Due to the units of five random variables not being unified and the corresponding orders of magnitude of the five input variables being different, the sensitivity standardization calculation is required. After standardized distribution parameters  $\mu_{X_i}$  and  $\sigma_{X_i}$ , the corresponding sensitivity can be expressed as Equation (22) [42,43].

$$\begin{aligned} S_{\mu_{X_i}} &= \frac{\partial P_f}{\partial \mu_{X_i}} \frac{\sigma_{X_i}}{P_f} \\ S_{\sigma_{X_i}} &= \frac{\partial P_f}{\partial \sigma_{X_i}} \frac{\sigma_{X_i}}{P_f} \end{aligned} \tag{22}$$

The reliability sensitivity gradient of the  $i$ -th random variable to  $P_f$  is:

$$S_i = \sqrt{S_{\mu_{X_i}}^2 + S_{\sigma_{X_i}}^2} \tag{23}$$

The sensitivity factor of the RPC-FST system can be obtained by standardizing the gradient of five parameters, as given in Equation (24).

$$\lambda_i = \frac{S_i}{\sum_{k=1}^{N_{MC}} S_k} \times 100\% \tag{24}$$

where  $N_{MC}$  is the number of sample pools.

#### 4.3. Sensitivity Analysis of the RPC-FST

Based on a numerical example provided in Section 3, 20 sample groups are selected to establish the Kriging surrogate model. The accuracy of the Kriging surrogate model needs to be verified, so 10 groups of data obtained by numerical calculation are used as verification groups and standard values. Absolute error  $E_A$  and relative error-index  $\beta_R$  are critical parameters for evaluating the response surface. The design of the experiment is shown in Table 9. The Bayesian method can update the coefficient of variation based on samples. It should be pointed out that coefficients of variation can be obtained in large-scale tests [44]. The distribution of random variables is shown in Table 10. These numerical examples are tested on a personal computer with Intel i7-9700 and 16 GB memory. The analysis structure of the relative error-index is shown in Table 11. The data shows that the error fluctuates within an acceptable range. It confirmed that the derived Kriging surrogate model could predict the displacement of the RPC-FST accurately. The Kriging surrogate model constructed by the limit state function is used for calculation. Furthermore,  $10^6$  MCS is used to calculate the reliability sensitivity prognosis of the RPC-FST system [45].

**Table 9.** Design of experiment.

Variable	Lower Bound	Upper Bound	Unit
TNT weight $W$	150	300	kg
Distance of TNT $L$	1000	2000	mm
Diameter of RPC-FST $D$	300	500	mm
Thickness of steel tube $t$	10	20	mm
Height of RPC-FST $H$	2000	3000	mm

**Table 10.** Distribution of random variables.

Variable	Distribution	Mean	Variable Coefficient	Unit
$W$	normal	225	0.01	kg
$L$	normal	1500	0.001	mm
$D$	normal	400	0.01	mm
$t$	normal	15	0.1	mm
$H$	normal	2500	0.001	mm

**Table 11.** Testing results based on testing samples.

$N$	$W$ (kg)	$L$ (m)	$D$ (mm)	$T$ (mm)	$H$ (mm)	$g_L(X_L)$ (mm)	$g_k(X_L)$ (mm)	$E_A$	$\beta_R$
1	278.98	1.57	318.33	18.90	2516.67	16.00	14.91	−1.09	−0.07
2	149.32	1.82	338.67	12.50	2333.67	18.40	17.99	−0.41	−0.02
3	154.46	1.85	446.75	15.67	2798.33	2.73	3.00	0.26	0.10
4	245.45	1.17	371.67	15.70	2450.00	21.01	19.43	−1.58	−0.08
5	255.15	1.50	335.00	15.30	2216.67	18.72	19.82	1.10	0.06
6	224.02	1.23	461.67	17.90	2950.00	7.16	6.76	−0.40	−0.06
7	175.75	1.37	358.33	14.90	2416.67	18.16	17.74	−0.41	−0.02
8	166.05	1.10	421.67	18.10	2016.67	10.93	9.47	−1.46	−0.13
9	236.95	1.90	368.33	19.10	2650.00	5.68	6.50	0.82	0.15
10	240.18	1.17	495.00	14.30	2183.33	20.19	19.21	−0.98	−0.05

From Figure 8a, it is obvious that the overall maximum displacement of RPC-FST has a greater correlation with the five variables of steel tube thickness, RPC-FST column height, TNT weight, TNT distance, and RPC-FST section diameter. However, the positive and negative correlations of the five variables with RPC-FST maximum displacement are different. The maximum displacement risk of RPC-FST increases with the increase of TNT weight and RPC-FST column height (positive correlation) and increases with the decrease of RPC-FST section diameter, steel tube thickness, and TNT distance (negative correlation). This can be concluded from Figure 8b.

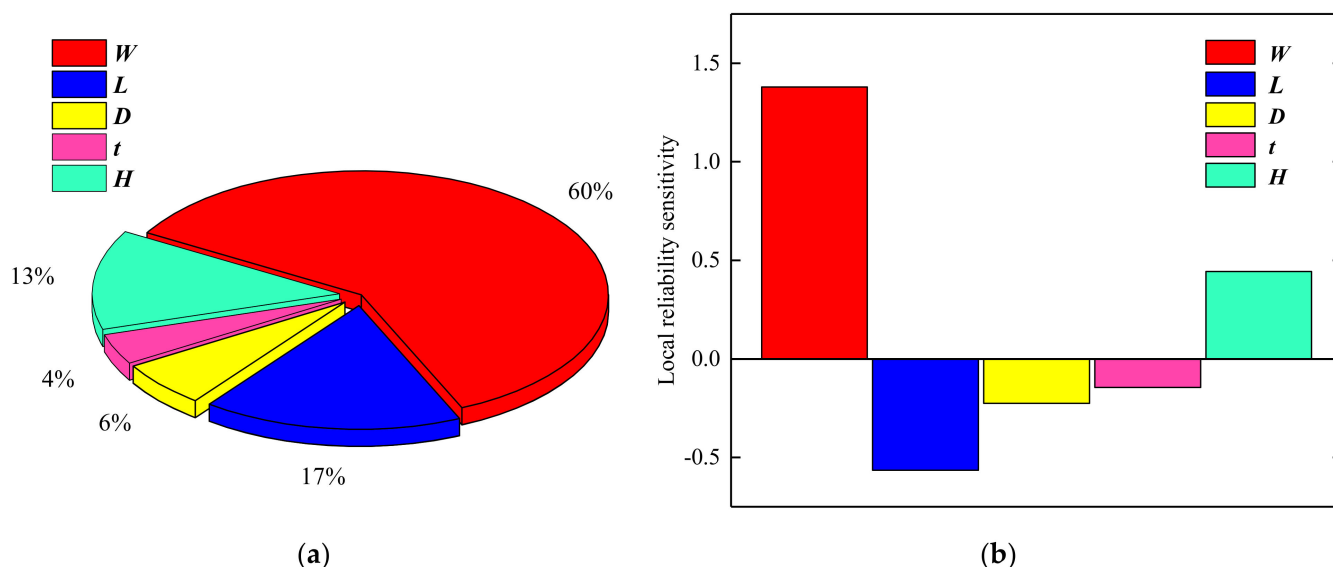


Figure 8. (a) Sensitivity factor of each parameter and (b) local reliability sensitivity of each parameter.

To compare the efficiency of the three models (the modified HJC model, the modified K&C model, and the Kriging surrogate model) in calculating the maximum displacement, we selected four sets of data for analysis, as shown in Table 11. The results show that the updated Kriging surrogate model in this paper can significantly improve the sensitivity analysis efficiency of the RPC-FST system under explosion load, as shown in Table 12.

Table 12. Efficiency competitions of three models.

Testing Sample	Total CPU Time (s)		
	Modified HJC Model	Modified K&C Model	Kriging Surrogate Model
1	9562	15,423	67
2	15,447	19,661	70
3	11,212	15,223	62
4	11,329	18,195	69

### 5. Conclusions

The displacement prediction model of RPC-FST under random explosion load is established based on fluid–solid interaction (FSI) theory. The main conclusions are as follows:

(1) The modified K&C model has higher accuracy than the modified HJC model in calculating the dynamic response of RPC-FST columns under explosion load. This is mainly because the previous HJC model is applicable to RPC materials with coarse aggregate and porosity of 10.5%. Although the HJC model is calibrated by modifying the porosity and related parameters, a lack of test for the ultimate strain of RPC (*EFMIN*) caused the calculated deflection to be lower than the test deflection in the modified HJC model.

(2) It takes a long time to use the ALE method to carry out the numerical calculations under RPC-FST explosion loading. The updated Kriging surrogate model can significantly

shorten the required time for the FSI theoretical analysis by more than 200 times. Besides, the RPC-FST dynamic response analysis based on the updated Kriging surrogate model has high accuracy.

(3) Based on the analysis of the five random parameters by the Kriging surrogate model, the TNT weight has the most significant impact on the risk of maximum displacement of RPC-FST compared with other parameters.

**Author Contributions:** Z.J.: investigation, software, formal analysis, original draft, writing—review and editing. Q.R.: investigation, methodology, software, formal analysis, funding acquisition, writing—review and editing. X.H.: methodology, formal analysis, writing—review and editing, funding acquisition. Z.Z.: investigation, software, writing—review and editing. E.Y.: writing—review and editing. All authors have read and agreed to the published version of the manuscript.

**Funding:** This research was funded by the Excellent Youth Foundation of Heilongjiang Province: No. YQ2019E028; National Natural Science Foundation of China: No. 52078169; Outstanding Young Talents Project of Harbin University of Science and Technology: LGYC2018JQ018.

**Acknowledgments:** This contribution is supported by the National Natural Science Foundation of China (No. 52078169), Excellent Youth Foundation of Heilongjiang Province (No. YQ2019E028), and Outstanding Young Talents Project of Harbin University of Science and Technology (LGYC2018JQ018).

**Conflicts of Interest:** The authors declare no conflict of interest.

## Nomenclature

$W$	TNT weight
$L$	TNT distance
$H$	RPC-FST height
$D$	RPC-FST section diameter
$t$	Steel tube thickness
$a_0, a_1, a_2$	Failure surface parameter
$B_1$	Compressive damage parameter
$B_2$	Tensile damage scaling exponent
$B_3$	Damage scaling coefficient
$a_{0y}, a_{1y}, a_{2y}$	Initial yield surface coefficient
$a_{1f}, a_{2f}$	Residual failure surface coefficient
$\eta_1\text{--}\eta_{13}$	Damage function
$\lambda_1\text{--}\lambda_{13}$	Scale factor
$\varepsilon_{v1}\text{--}\varepsilon_{v10}$	Volumetric strain
$C_1\text{--}C_{10}$	Mechanical pressure
$T_1\text{--}T_{10}$	Temperature parameter
$K_1\text{--}K_{10}$	Bulk unloading modulus
$A, B, R_1, R_2, \omega$	Parameters of TNT
$\varepsilon(x)$	Maximum displacement based on FSI theory
$\theta$	Deflection angle of RPC-FST
$P_f$	Failure probability
$I_F(X)$	Indication function of the failure domain

## Appendix A. Modified HJC Model

The HJC model is a constitutive model proposed by Holmquist [46], which solves the problem of large deformation of concrete under high strain rate. At present, the HJC material model is widely used in the dynamic impact failure process of UHPCs [14,16,47]. Therefore, the applicability of the HJC model for RPC needs to be further discussed.

The HJC constitutive model mainly includes three parts: the equation of yield surface, equation of damage evolution, and equation of state. The damage evolution equation and state equation of the HJC model will be modified. The parameters of yield surface equation are modified by Wan [14]. The modification of yield surface equation will not be explained here. The modified HJC model process is shown in Figure A1.

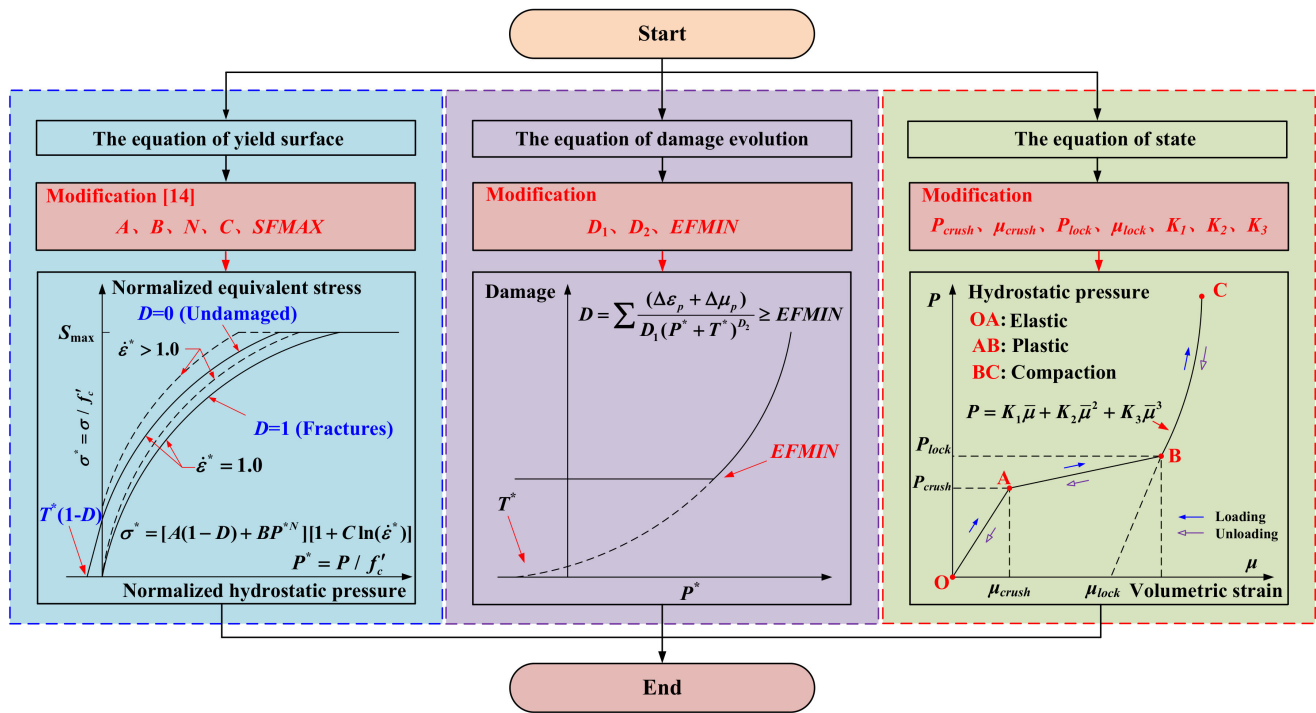


Figure A1. Modified HJC model process.

The damage evolution equation considers the damage of equivalent plastic strain and plastic volume strain. The damage parameter can be expressed as:

$$D = \sum \frac{\Delta \epsilon_p + \Delta \mu_p}{D_1(P^* + T^*)^{D_2}} \geq EFMIN \tag{A1}$$

where  $\Delta \epsilon_p$  and  $\Delta \mu_p$  are the equivalent plastic strain and plastic volumetric strain;  $P^*$  and  $T^*$  are the normalized hydrostatic pressure and the normalized maximum tensile hydrostatic pressure; and  $D_1, D_2$ , and  $EFMIN$  are the key parameters constituting the damage evolution equation. Assume  $D_2$  as 1.0, and  $EFMIN = \epsilon_x$  [46].  $D_1$  is expressed as:

$$D_1 = \frac{EFMIN}{1/6 + T^*} = \frac{\epsilon_x}{1/6 + T^*} \tag{A2}$$

According to the parameter determination method [46], it is considered that the ultimate strain  $\epsilon_x$  can be obtained through uniaxial compression tests. Therefore, the assumed failure surface is determined through Prabha and Prem's [48,49] test, and the ultimate strain value is obtained based on the assumed failure surface. The results are shown in Figure A2. The  $D_1$  value is obtained by Equation (A2), as shown in Table A1. It should be noted that Wan [14] determined the damage parameters of different steel fiber contents according to specimens 1, 2, 3, and 8 (Table A1). However, through the analysis of specimens 4, 5, 6, and 7 (Table A1), it is found that the damage constant  $D_1$  has a certain relationship with steel fiber length and water/cement ratio (W/C). The results show that when the steel fiber content is 2% (specimen 3, 4, 5), increase of the water/cement ratio will lead to a decrease of  $EFMIN$  and  $D_1$ , and an increase in steel fiber length will lead to an increase of  $EFMIN$  and  $D_1$ . Therefore, the values of the  $EFMIN$  and  $D_1$  parameters are modified. In addition, this provides a reference for values under other working conditions.

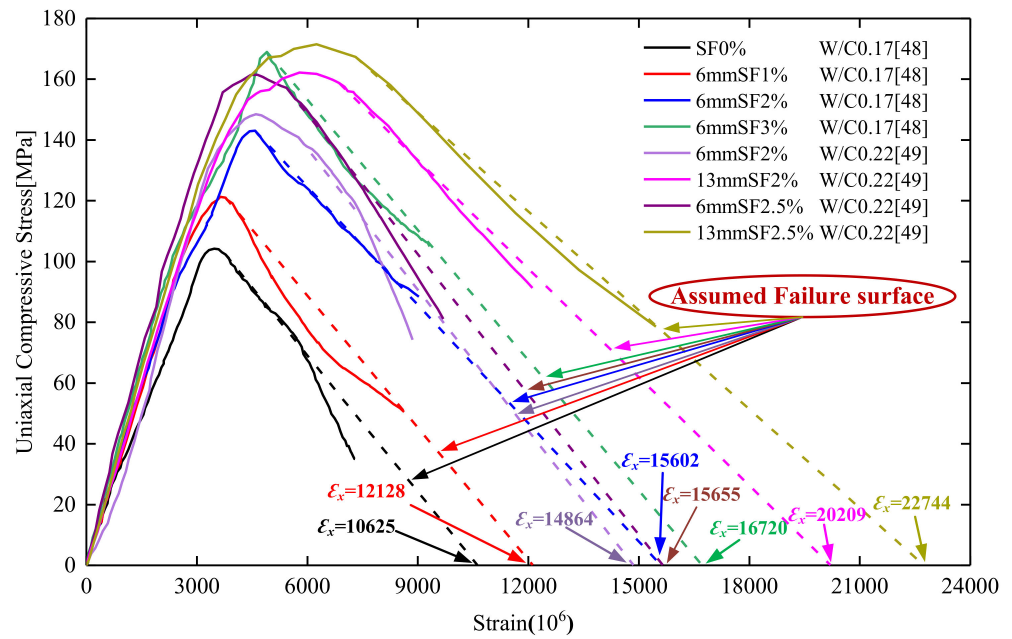


Figure A2. The ultimate strains ( $\epsilon_x$ ) of specimens.

Table A1. Parameters of damage evolution equation.

Specimen	1	2	3	4	5	6	7	8
Steel fiber content	0%	1%	2%	2%	2%	2.5%	2.5%	3%
Steel fiber length	0 mm	6 mm	6 mm	6 mm	13 mm	13 mm	6 mm	6 mm
W/C	0.17	0.17	0.17	0.22	0.22	0.22	0.22	0.17
$D_1$	0.045	0.05	0.061	0.054	0.067	0.077	0.057	0.063
$EFMIN$	0.011	0.012	0.016	0.015	0.02	0.023	0.016	0.017

The equation of state describes the relationship between hydrostatic pressure  $P$  and volumetric strain  $\mu$  through three stages. In addition,  $P_{crush}$ ,  $\mu_{crush}$ ,  $P_{lock}$ ,  $\mu_{lock}$ ,  $K_1$ ,  $K_2$ , and  $K_3$  define the equation of state. It can be expressed as:

$$P = \begin{cases} K_{elastic}\mu & P \leq P_{crush} \text{ Elastic} \\ \frac{P_{crush}-P_{lock}}{\mu_{crush}-\mu_{plock}}(\mu - \mu_{crush}) + P_{crush} & P_{crush} < P < P_{lock} \text{ Plastic} \\ K_1\bar{\mu} + K_2\bar{\mu}^2 + K_3\bar{\mu}^3 & P \geq P_{lock} \text{ Compaction} \end{cases} \quad (A3)$$

where  $K_{elastic} = P_{crush} / \mu_{crush}$  is the elastic bulk modulus,  $\bar{\mu} = (\mu - \mu_{lock}) / (1 + \mu_{lock})$  is the modified volumetric strain, and  $\mu_{plock}$  is the volume strain of the material at  $P_{lock}$ .  $P_{crush}$  and  $\mu_{crush}$  can be expressed as:

$$P_{crush} = f'_c / 3 \quad (A4)$$

$$\mu_{crush} = 0.6f'_c / E \quad (A5)$$

where  $E$  is the elastic modulus.

Considering that the porosity of RPC without coarse aggregate is about 5% [50], the parameters of the HJC state equation are modified.  $\mu_{lock} = \rho_{grain} / \rho_0 - 1$ , and  $1 - \rho_0 / \rho_{grain} = 0.05$ .  $\rho_{grain}$  is the grain density.  $\rho_0$  is the initial density. So far,  $P_{crush}$ ,  $\mu_{crush}$ , and  $\mu_{lock}$  can be determined. The modified parameters  $P_{lock}$ ,  $K_1$ ,  $K_2$ , and  $K_3$  are obtained from the Hugoniot test data of Gebbeken [51], as shown in Figure A3. The results show that when the porosity is low, the material will reach the compaction stage ahead of time.

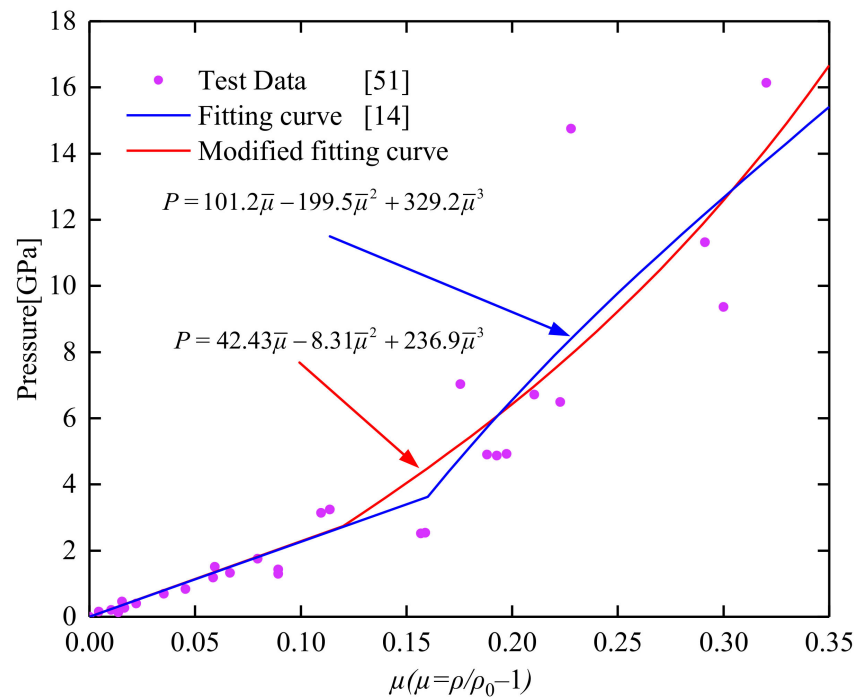


Figure A3. Comparison of fitting curves under different porosity.

In the experiment [33], the water/cement ratio is 0.22, and the steel fiber content is 2%. The modified HJC model parameters are applied to Section 3, as shown in Table A2.

Table A2. Modified HJC model parameters.

Parameter	Value	Parameter	Value
Mass density $R_0$ (g/mm <sup>3</sup> )	$2.40 \times 10^{-3}$	Shear modulus $G$ (MPa)	17,875
Normalized cohesive strength $A$	0.3	Normalized pressure hardening $B$	1.781
Strain rate coefficient $C$	0.019	Pressure hardening exponent $N$	0.81
Compressive strength	135.1	Tensile pressure $T$ (MPa)	9
Strain rate $EPS0$ (ms <sup>-1</sup> )	0.001	Plastic strain $EFMIN$	0.015
Maximum strength $SFMAX$	3.5	Crushing pressure $P_{crush}$ (MPa)	45.03
Crushing volumetric strain $\mu_{crush}$	0.00189	Locking pressure $P_{lock}$ (MPa)	2743.65
Damage constant $D_1$	0.054	Damage constant $D_2$	1
Pressure constant $K_1$ (MPa)	42430	Pressure constant $K_2$ (MPa)	-8310
Pressure constant $K_3$ (MPa)	236900	Failure type $FS$	0.1
Locking volumetric strain $\mu_{lock}$	0.053		

References

- Hinman, E. Primer for design of commercial buildings to mitigate terrorist attacks. In *Risk Management Series FEMA*; Federal Emergency Management Agency: Washington, DC, USA, 2003.
- Chipley, M.; Lyon, W.; Smilowitz, R.; Williams, P.; Arnold, C.; Blewett, W.; Hazen, L.; Krimgold, F. *Primer to Design Safe School Projects in Case of Terrorist Attacks and School Shootings, Buildings and Infrastructure Protection Series*; FEMA-428/BIPS-07/January 2012; US Department of Homeland Security: Washington, DC, USA, 2012.
- TM5-1300. *Structures to Resist the Effects of Accidental Explosions*; US Department of the Army: Washington, DC, USA, 1990.
- Reifarh, C.; Castedo, R.; Santos, A.; Chiquito, M.; López, L.; Pérez-Caldentey, A.; Martínez-Almajano, S.; Alañon, A. Numerical and experimental study of externally reinforced RC slabs using FRPs subjected to close-in blast loads. *Int. J. Impact Eng.* **2021**, *156*, 103939. [CrossRef]
- Do, T.V.; Pham, T.M.; Hao, H. Stress Wave Propagation and Structural Response of Precast Concrete Segmental Columns under Simulated Blast Loads. *Int. J. Impact Eng.* **2020**, *143*, 103595. [CrossRef]

6. Ritchie, C.B.; Packer, J.A.; Seica, M.V.; Zhao, X.-L. Behaviour and analysis of concrete-filled rectangular hollow sections subject to blast loading. *J. Constr. Steel Res.* **2018**, *147*, 340–359. [[CrossRef](#)]
7. Abedini, M.; Zhang, C.; Mehrmashhadi, J.; Akhlaghi, E. Comparison of ALE, LBE and pressure time history methods to evaluate extreme loading effects in RC column. *Structures* **2020**, *28*, 456–466. [[CrossRef](#)]
8. Thai, D.-K.; Nguyen, D.-L.; Pham, T.-H.; Doan, Q.H. Prediction of residual strength of FRC columns under blast loading using the FEM method and regression approach. *Constr. Build. Mater.* **2021**, *276*, 122253. [[CrossRef](#)]
9. Kostopoulos, V.; Kalimeris, G.D.; Giannaros, E. Blast protection of steel reinforced concrete structures using composite foam-core sacrificial cladding. *Compos. Sci. Technol.* **2022**, 109330. [[CrossRef](#)]
10. Wu, H.; Peng, Y.L.; Fang, Q. Experimental and numerical study of ultra-high performance cementitious composites filled steel tube (UHPCC-FST) subjected to close-range explosion. *Int. J. Impact Eng.* **2020**, *141*, 103569. [[CrossRef](#)]
11. Kong, X.; Fang, Q.; Chen, L.; Wu, H. A new material model for concrete subjected to intense dynamic loadings. *Int. J. Impact Eng.* **2018**, *120*, 60–78. [[CrossRef](#)]
12. Zhu, Q.-F.; Huang, Z.-X.; Xiao, Q.-Q.; Zu, X.-D.; Jia, X.; Ma, B. Theoretical considerations on cavity diameters and penetration depths of concrete materials generated by shaped charge jets using the targets response modes described by a modified HJC model. *Int. J. Impact Eng.* **2020**, *138*, 103439. [[CrossRef](#)]
13. Kristoffersen, M.; Toreskås, O.L.; Dey, S.; Børvik, T. Ballistic perforation resistance of thin concrete slabs impacted by ogive-nose steel projectiles. *Int. J. Impact Eng.* **2021**, *156*, 103957. [[CrossRef](#)]
14. Wan, W.; Yang, J.; Xu, G.; Liu, Y. Determination and evaluation of Holmquist-Johnson-Cook constitutive model parameters for ultra-high-performance concrete with steel fibers. *Int. J. Impact Eng.* **2021**, *156*, 103966. [[CrossRef](#)]
15. Hallquist, J.O. LS-DYNA keyword user's manual. *Livermore Softw. Technol. Corp.* **2007**, *970*, 299–800.
16. Wang, Z.; Wu, H.; Fang, Q.; Wu, J. Numerical study on the residual axial capacity of ultra high performance cementitious composite filled steel tube (UHPCC-FST) column under contact explosion. *Thin-Walled Struct.* **2020**, *153*, 106832. [[CrossRef](#)]
17. Liu, L.; Zong, Z.; Gao, C.; Yuan, S.; Lou, F. Experimental and numerical study of CFRP protective RC piers under contact explosion. *Compos. Struct.* **2020**, *234*, 111658. [[CrossRef](#)]
18. Zhang, F.; Shedbale, A.S.; Zhong, R.; Poh, L.H.; Zhang, M.-H. Ultra-high performance concrete subjected to high-velocity projectile impact: Implementation of K&C model with consideration of failure surfaces and dynamic increase factors. *Int. J. Impact Eng.* **2021**, *155*, 103907.
19. Xu, X.; Zhang, R.H.; Liu, Y.H. Influence of curing regime on properties of reactive powder concrete containing waste steel fibers. *Constr. Build. Mater.* **2020**, *232*, 117129.
20. Chen, M.Y.; Hou, X.M. Comparative study on the axial compression and bearing capacity of reactive powder concrete-filled circular steel tube. *Adv. Mater. Sci. Eng.* **2018**, *2018*, 8038649. [[CrossRef](#)]
21. Chen, W.; Luo, L.; Guo, Z.; Zou, H. Strain rate effects on dynamic strength of high temperature-damaged RPC-FST. *J. Constr. Steel Res.* **2018**, *147*, 324–339. [[CrossRef](#)]
22. Chen, W.; Pan, J.; Guo, Z.; Zou, H. Damage evaluations of fire-damaged RPC-FST columns under blast loading. *Thin-Walled Struct.* **2019**, *134*, 319–332. [[CrossRef](#)]
23. Hussein, A.; Mahmoud, H.; Heyliger, P. Probabilistic analysis of a simple composite blast protection wall system. *Eng. Struct.* **2020**, *203*, 109836. [[CrossRef](#)]
24. Song, X.R. Parameterized fragility analysis of steel frame structure subjected to blast loads using Bayesian logistic regression method. *Struct. Saf.* **2020**, *87*, 102000. [[CrossRef](#)]
25. Ding, Y.; Song, X.R.; Zhu, H.T. Probabilistic progressive collapse analysis of steel frame structures against blast loads. *Eng. Struct.* **2017**, *147*, 679–691. [[CrossRef](#)]
26. Shi, Y.F.; Stewart, M.G. Damage and risk assessment for reinforced concrete wall panels subjected to explosive blast loading. *Int. J. Impact Eng.* **2015**, *85*, 5–19. [[CrossRef](#)]
27. Momeni, M.; Bedon, C.; Hadianfard, M.A.; Baghlani, A. An efficient reliability-based approach for evaluating safe scaled distance of steel columns under dynamic blast loads. *Buildings* **2022**, *11*, 606. [[CrossRef](#)]
28. Li, M.; Zong, Z.; Hao, H.; Zhang, X.; Lin, J.; Xie, G. Experimental and numerical study on the behaviour of CFDST columns subjected to close-in blast loading. *Eng. Struct.* **2019**, *185*, 203–220. [[CrossRef](#)]
29. Richard, P.; Cheyrezy, M. Composition of reactive powder concretes. *Cem. Concr. Res.* **1995**, *25*, 1501–1511. [[CrossRef](#)]
30. Cao, S.J.; Hou, X.M.; Rong, Q. Dynamic compressive properties of reactive powder concrete at high temperature: A review. *Cem. Concr. Compos.* **2020**, *110*, 103568. [[CrossRef](#)]
31. Rong, Q.; Hou, X.M.; Ge, C. Quantifying curing and composition effects on compressive and tensile strength of 160-250 MPa RPC. *Constr. Build. Mater.* **2020**, *241*, 117987. [[CrossRef](#)]
32. Hou, X.; Cao, S.; Zheng, W.; Rong, Q.; Li, G. Experimental study on dynamic compressive properties of fiber-reinforced reactive powder concrete at high strain rates. *Eng. Struct.* **2018**, *169*, 119–130. [[CrossRef](#)]
33. Wang, Z.G.; Wu, H.; Sun, Y.Y. Experimental study on residual seismic behavior of UHPCC-FST after near-range explosion. *Structures* **2021**, *32*, 1428–1443. [[CrossRef](#)]
34. Chen, S.; Hou, C.; Zhang, H.; Han, L.-H. Structural behaviour and reliability of CFST trusses with random initial imperfections. *Thin-Walled Struct.* **2019**, *143*, 106192. [[CrossRef](#)]

35. Li, G.; Hou, C.; Shen, L.; Yao, G.-H. Performance and strength calculation of CFST columns with localized pitting corrosion damage. *J. Constr. Steel Res.* **2022**, *188*, 107011. [[CrossRef](#)]
36. Hou, X.; Cao, S.; Rong, Q.; Zheng, W. A P-I diagram approach for predicting failure modes of RPC one-way slabs subjected to blast loading. *Int. J. Impact Eng.* **2018**, *120*, 171–184. [[CrossRef](#)]
37. Li, S.J.; Huang, X.Z.; Wang, D.H. Stochastic configuration networks for multi-dimensional integral evaluation. *Inf. Sci.* **2022**, *601*, 323–339. [[CrossRef](#)]
38. Jia, D.W.; Wu, Z.Y. A Laplace asymptotic integral-based reliability analysis method combined with artificial neural network. *Appl. Math. Model.* **2022**, *105*, 406–422. [[CrossRef](#)]
39. Li, Y.; Wu, Y.; Zhang, Y.; Wang, S. A Kriging-based bi-objective constrained optimization method for fuel economy of hydrogen fuel cell vehicle. *Int. J. Hydrog. Energy* **2019**, *44*, 29658–29670. [[CrossRef](#)]
40. Davidson, P.; Waas, A.M. Probabilistic defect analysis of fiber reinforced composites using kriging and support vector machine based surrogates. *Compos. Struct.* **2018**, *195*, 186–198. [[CrossRef](#)]
41. Jiang, Z.; Huang, X.; Chang, M.; Li, C.; Ge, Y. Thermal error prediction and reliability sensitivity analysis of motorized spindle based on Kriging model. *Eng. Fail. Anal.* **2021**, *127*, 105558. [[CrossRef](#)]
42. Wu, Y.T.; Mohanty, S. Variable screening and ranking using sampling-based sensitivity measures. *Reliab. Eng. Syst. Saf.* **2006**, *91*, 634–647. [[CrossRef](#)]
43. Mansour, A.E.; Wirsching, P.H. Sensitivity factors and their application to marine structures. *Mar. Struct.* **1995**, *8*, 229–255. [[CrossRef](#)]
44. Thangjai, W.; Niwitpong, S.A.; Niwitpong, S. A Bayesian Approach for Estimation of Coefficients of Variation of Normal Distributions. *Sains Malays.* **2021**, *50*, 261–278. [[CrossRef](#)]
45. Zhang, X.; Lu, Z.; Cheng, K.; Wang, Y. A novel reliability sensitivity analysis method based on directional sampling and Monte Carlo simulation, Proceedings of the Institution of Mechanical Engineers. *Part J. Risk Reliab.* **2020**, *234*, 622–635.
46. Holmquist, T.J.; Johnson, G.R.; Cook, W.H. A computational constitutive model, for concrete subjected to large strains, high strain rates, and high pressures. In Proceedings of the 14th International Symposium on Ballistic, Quebec city, QC, Canada, 26–29 September 1993; pp. 591–600.
47. Zhai, Y.X.; Wu, H.; Fang, Q. Impact resistance of armor steel/ceramic/UHPC layered composite targets against 30CrMnSiNi2A steel projectiles. *Int. J. Impact Eng.* **2021**, *154*, 103888. [[CrossRef](#)]
48. Prabha, S.L.; Dattatreya, J.K.; Neelamegam, M.; Seshagirirao, M.V. Study on stress-strain properties of reactive powder concrete under uniaxial compression. *Int. J. Eng. Sci. Technol.* **2010**, *2*, 6408–6416.
49. Prem, P.R.; Murthy, A.R.; Bharatkumar, B.H. Influence of curing regime and steel fibres on the mechanical properties of UHPC. *Mag. Concr. Res.* **2015**, *67*, 1400333. [[CrossRef](#)]
50. Abid, M.; Hou, X.; Zheng, W.; Hussain, R.R. Effect of fibers on high-temperature mechanical behavior and microstructure of reactive powder concrete. *Materials* **2019**, *12*, 329. [[CrossRef](#)]
51. Gebbeken, N.; Greulich, S.; Pietzsch, A. Hugoniot properties for concrete determined by full-scale detonation experiments and flyer-plate-impact tests. *Int. J. Impact Eng.* **2006**, *32*, 2017–2031. [[CrossRef](#)]